Parton content of virtual photons

M. Glück, E. Reya, and M. Stratmann
Institut für Physik, Universität Dortmund, D-44221 Dortmund, Federal Republic of Germany
(Received 12 August 1994)

The parton content of virtual transverse photons $\gamma(P^2)$ is expressed in terms of perturbative pointlike and nonperturbative hadronic (VMD) components. The resulting LO and NLO parton distributions $f^{\gamma(P^2)}(x,Q^2)$ are *smooth* in P^2. They apply uniformly to *all* $P^2 \geq 0$ whenever $\gamma(P^2)$ is probed at a scale $Q^2 \gg P^2$ where the transverse photons furthermore also dominate physically relevant cross sections. Predictions are given for $F_2^{\gamma(P^2)}(x,Q^2)$ and $u^{\gamma(P^2)}(x,Q^2)$, $g^{\gamma(P^2)}(x,Q^2)$ relevant for future CERN LEP and present DESY HERA measurements, respectively. Except for certain kinematic regions, these virtual structure functions and parton distributions at $\Lambda^2 \ll P^2 \ll Q^2$ are *not* solely described by purely perturbative contributions, in contrast with "naive" expectations; these remaining nonperturbative components, although being based on VMD-inspired simplicity, represent the largest uncertainty in our quantitative results and eventually have to be tested by future experiments.

PACS number(s): 13.60.Hb, 12.38.Bx, 13.65.+i, 14.70.Bh

I. INTRODUCTION

High energy electrons at, say, e^+e^- or ep colliders produce a flux of transverse photons whose virtuality is determined by tagging the outgoing electron(s). For clarity let us denote the target photon with virtuality $P^2 \equiv -p_\gamma^2$ by $\gamma(P^2)$ which is probed by the virtual probe photon $\gamma^*(Q^2), Q^2 \equiv -q^2$, via the subprocess $\gamma^*(Q^2)\gamma(P^2) \to X$ as in $e^+e^- \to e^+e^-X$. One expects $\gamma(P^2)$ to possess a parton content $f^{\gamma(P^2)}(x,Q^2), f = q, \bar{q}, g$, which is expected [1,2] to be perturbatively calculable for $\Lambda^2 \ll P^2 \ll Q^2$. For P^2 approaching Q^2, $P^2 \simeq Q^2$, the e^+e^- results should reduce to the one given by the full quark parton model (QPM) box $\gamma^*(Q^2)\gamma(P^2) \to q\bar{q}$ with possible higher twist (P^2/Q^2) terms and $O(\alpha_s)$ corrections included, whereas the usual parton distributions of real photons, $f^\gamma(x,Q^2)$, are encountered for $P^2 = 0$. It should be noted that these virtual photonic parton distributions can and will be tested in tagged $ep \to eX$ collisions via the subprocess $\gamma(P^2)p \to X$, where now the scale Q in $f^{\gamma(P^2)}(x,Q^2)$ refers to some properly chosen scale of the produced hadronic system X, e.g., $Q \sim p_T^{\text{jet}}$ in high-p_T ($p_T^2 \gg P^2$) jet events, etc.

It is the main purpose of the present paper to formulate a consistent set of boundary conditions which allow for a calculation of $f^{\gamma(P^2)}(x,Q^2)$ also in the next-to-leading order QCD *as well as* for a smooth transition to $P^2 = 0$, i.e., to the parton distributions of a real photon. Furthermore, in contrast with the expectations in [1,2] it will turn out that all predictions for virtual photonic parton distributions $f^{\gamma(P^2)}(x,Q^2)$ and structure functions $F_2^{\gamma(P^2)}(x,Q^2)$, relevant for present and future experiments at the DESY ep collider HERA and the CERN e^+e^- collider LEP, are *not* solely described by purely perturbative contributions at $\Lambda^2 \ll P^2 \ll Q^2$ and that the nonpointlike hadronic [vector meson dominance (VMD)] contributions are important in the small-x region, $x \ll 1$, for all relevant P^2 within $\Lambda^2 \ll P^2 \ll Q^2$, except for certain (extreme) kinematic regions.

II. THEORETICAL FRAMEWORK

A flux of transverse photons produced by high energy electrons at, say e^+e^- or ep colliders is given by [3]

$$\gamma^e(y) = \frac{\alpha}{2\pi}\left[\frac{1+(1-y)^2}{y}\ln\frac{P^2_{\max}}{P^2_{\min}} - 2m_e^2 y\left(\frac{1}{P^2_{\min}} - \frac{1}{P^2_{\max}}\right)\right], \tag{1}$$

where $y = E_\gamma/E_e$, $P^2 = -p_\gamma^2$, and where $P^2_{\min,\max}$ are determined by an eventual tagging of the outgoing electron e' at the photon producing vertex $e \to e'\gamma$. The range of photon masses produced is

$$m_e^2 y^2/(1-y) \leq P^2_{\min} \leq P^2 \leq P^2_{\max} \leq \frac{s}{2}(1-y)(1-\cos\theta_{\max}), \tag{2}$$

where s is the squared c.m. energy of the eX system in $eX \to e'X'$ and $\theta_{\max}$ is the maximal scattering angle of e' in this c.m. system. Since the bulk of the produced photons comes from the region $P^2 \simeq P^2_{\min}$, it is $P^2_{\min}$ which measures the photon virtuality involved, just as $P^2_{\min} = m_e^2 y^2/(1-y) \simeq 0$ in untagged or antitagging experiments is considered to represent real massless photons. For the transverse virtual target photons $\gamma(P^2)$, whose virtuality P^2 is essentially given by $P^2 \simeq P^2_{\min}$ and whose flux is approximated in (1), one expects a parton content $f^{\gamma(P^2)}(x,Q^2)$, where $f^{\gamma(P^2)} = (q^{\gamma(P^2)} =$

$\bar{q}^{\gamma(P^2)}, g^{\gamma(P^2)}$), at least for $P^2 \ll Q^2$. These distributions obey the same Q^2 evolution, i.e., renormalization group, equations as the real photon [$\gamma \equiv \gamma(P^2 = 0)$] distributions $f^\gamma(x, Q^2)$.

For $P^2 = 0$, i.e., *real* photons it has been shown in [4] that an appropriate prescription for the boundary conditions at the input scale $Q^2 = \mu^2$ is given by

$$f^\gamma(x, \mu^2) = \kappa(4\pi\alpha/f_\rho^2) f^\pi(x, \mu^2) \tag{3}$$

with κ, f_ρ^2, μ^2, and $f^\pi(x, \mu^2)$ given in [4] and [5], respectively. This is expected to hold for the leading order (LO) distributions as well as for the next-to-leading order (NLO) distributions in the deep inelastic scattering (DIS_γ) factorization scheme for photons [6] which are related to the modified minimal subtraction ($\overline{\mathrm{MS}}$) factorization scheme distributions via [4,6]

$$f^\gamma_{\mathrm{DIS}_\gamma}(x, Q^2) = f^\gamma_{\overline{\mathrm{MS}}}(x, Q^2) + \delta f^\gamma(x) \tag{4}$$

with

$$\begin{aligned}\delta q^\gamma(x) &= \delta \bar{q}^\gamma(x) \\ &= 3e_q^2 \frac{\alpha}{2\pi}\left\{[x^2 + (1-x)^2]\ln\frac{1-x}{x} - 1 \right. \\ &\qquad \left. + 8x - 8x^2\right\} \\ \delta g^\gamma(x) &= 0. \end{aligned} \tag{5}$$

For $P^2 \neq 0$, i.e., *virtual* photons, in particular for $P^2 \gg \Lambda^2$, the boundary conditions for $f^{\gamma(P^2)}(x, Q^2)$ at $Q^2 = P^2$ are perturbatively calculable and given by [1,2]

$$f^{\gamma(P^2)}_{\mathrm{LO}}(x, Q^2 = P^2) = 0 \tag{6}$$

or

$$\begin{aligned} q^{\gamma(P^2)}_{\mathrm{NLO}}(x, Q^2 = P^2) &= \bar{q}^{\gamma(P^2)}_{\mathrm{NLO}}(x, Q^2 = P^2) \\ &= 3e_q^2 \frac{\alpha}{2\pi}\left\{[x^2 + (1-x)^2]\ln\frac{1}{x^2} - 2 \right. \\ &\qquad \left. + 6x - 6x^2\right\}, \\ g^{\gamma(P^2)}_{\mathrm{NLO}}(x, Q^2 = P^2) &= 0 \end{aligned} \tag{7}$$

for a LO or NLO calculation under consideration. The NLO boundary conditions in (7) are again specified in the DIS_γ factorization scheme. It should be noted that the difference between the right hand sides (RHS) of Eqs. (5) and (7) is due to the fact that virtual photons with $P^2 \gg \Lambda^2$ exhibit, in contrast with real photons, a hard pointlike behavior which can be dealt with purely perturbatively [1,2] when calculating the virtual box $\gamma^*(Q^2)\gamma(P^2) \to q\bar{q}$ for $\Lambda^2 \ll P^2 \ll Q^2$.

A simple, VMD-inspired, smooth interpolation between Eq. (3), valid at $P^2 = 0$, and Eqs. (6) and (7), valid at $P^2 \gg \Lambda^2$, may be uniquely fixed by

$$\begin{aligned} f^{\gamma(P^2)}(x, Q^2 = \tilde{P}^2) &= \eta(P^2) f^{\gamma(P^2)}_{\mathrm{nonpert}}(x, \tilde{P}^2) \\ &\quad + [1 - \eta(P^2)] f^{\gamma(P^2)}_{\mathrm{pert}}(x, \tilde{P}^2) \end{aligned} \tag{8}$$

with $\tilde{P}^2 = \max(P^2, \mu^2)$ and

$$\eta(P^2) = (1 + P^2/m_\rho^2)^{-2}, \tag{9}$$

where, for definiteness, $m_\rho^2 = 0.59\ \mathrm{GeV}^2$ refers to some effective mass in the vector-meson propagator. Note that the ansatz in Eq. (8) implies that the input parton distributions are frozen at $Q^2 = \mu^2$ for $0 \le P^2 \le \mu^2$. Because of our present ignorance, we refrain from considering a more general [7] VMD ansatz. The perturbatively calculable input $f^{\gamma(P^2)}(x, \tilde{P}^2)$ in Eq. (8) is given by Eq. (6) or (7) for the LO or NLO distributions, respectively, and the hadronic nonperturbative one by

$$f^{\gamma(P^2)}_{\mathrm{nonpert}}(x, \tilde{P}^2) = \kappa(4\pi\alpha/f_\rho^2) \times \begin{cases} f^\pi(x, P^2), & P^2 > \mu^2, \\ f^\pi(x, \mu^2), & 0 \le P^2 \le \mu^2, \end{cases} \tag{10}$$

where $\mu^2_{\mathrm{LO}} = 0.25\ \mathrm{GeV}^2$ and $\mu^2_{\mathrm{NLO}} = 0.3\ \mathrm{GeV}^2$ refer to the LO and NLO input scales for the parton distributions of the real photon [4].

The flavor nonsinglet and singlet distributions $f^{\gamma(P^2)}(x, Q^2)$ obtained, according to these boundary conditions, from solving the NLO inhomogeneous Q^2-evolution equations are formally very similar to the ones of a real photon [6] and can be given analytically for (Mellin) n moments:

$$\begin{aligned} f^{\gamma(P^2),n}(Q^2) &\equiv \int_0^1 dx\, x^{n-1} f^{\gamma(P^2)}(x, Q^2) \\ &= f^{\gamma(P^2),n}_{\mathrm{pl}}(Q^2) + f^{\gamma(P^2),n}_{\mathrm{had}}(Q^2) \end{aligned} \tag{11}$$

with the "pointlike" (inhomogeneous) flavor-singlet solution [6]

$$\begin{aligned} \begin{pmatrix} \Sigma^{\gamma(P^2),n}_{\mathrm{pl}}(Q^2) \\ g^{\gamma(P^2),n}_{\mathrm{pl}}(Q^2) \end{pmatrix} &= \frac{4\pi}{\alpha_s(Q^2)}\left(1 + \frac{\alpha_s(Q^2)}{2\pi}\hat{U}\right)\left[1 - L^{1-(2/\beta_0)\hat{P}^{(0)n}}\right]\frac{1}{1 - \frac{2}{\beta_0}\hat{P}^{(0)n}}\frac{\alpha}{2\pi\beta_0}\vec{k}^{(0)n} \\ &\quad + \left[1 - L^{-(2/\beta_0)\hat{P}^{(0)n}}\right]\frac{1}{-\hat{P}^{(0)n}}\frac{\alpha}{2\pi}\left(\vec{k}^{(1)n} - \frac{\beta_1}{2\beta_0}\vec{k}^{(0)n} - \hat{U}\vec{k}^{(0)n}\right), \end{aligned} \tag{12}$$

where $\Sigma = \Sigma_f(q + \bar{q})$ and $\vec{k}^{(0)}$ and $\vec{k}^{(1)}$ denote the inhomogeneous LO and NLO photon splitting functions into quarks and gluons [6], and the "hadronic" (homogeneous) solution

$$\begin{pmatrix} \Sigma_{\rm had}^{\gamma(P^2),n}(Q^2) \\ g_{\rm had}^{\gamma(P^2),n}(Q^2) \end{pmatrix} = \left\{ L^{-(2/\beta_0)\hat{P}^{(0)n}} + \frac{\alpha_s(Q^2)}{2\pi}\hat{U}L^{-(2/\beta_0)\hat{P}^{(0)n}} - \frac{\alpha_s(\tilde{P}^2)}{2\pi}L^{-(2/\beta_0)\hat{P}^{(0)n}}\hat{U} \right\} \begin{pmatrix} \Sigma_{\rm had}^{\gamma(P^2),n}(\tilde{P}^2) \\ g_{\rm had}^{\gamma(P^2),n}(\tilde{P}^2) \end{pmatrix}, \quad (13)$$

where the 2×2 matrix $\hat{U}$ is expressed in terms of the 2×2 matrices of one- and two-loop splitting functions $\hat{P}^{(0)n}$ and $\hat{P}^{(1)n}$ as given in Ref. [6]. The input distributions $f_{\rm had}^{\gamma(P^2),n}(\tilde{P}^2) = f^{\gamma(P^2),n}(Q^2 = \tilde{P}^2)$ with $f^{\gamma(P^2)}(x, Q^2 = \tilde{P}^2)$ given by Eq. (8) and $L \equiv \alpha_s(Q^2)/\alpha_s(\tilde{P}^2)$, where

$$\frac{\alpha_s(Q^2)}{4\pi} \simeq \frac{1}{\beta_0 \ln Q^2/\Lambda^2} - \frac{\beta_1}{\beta_0^3}\frac{\ln\ln Q^2/\Lambda^2}{(\ln Q^2/\Lambda^2)^2} \quad (14)$$

with $\Lambda_{\rm LO} \simeq \Lambda_{\rm NLO} = 200$ MeV for $f = 4$ flavors. For $0 \le P^2 \le \mu^2$ one of course has to freeze $\alpha_s(\tilde{P}^2)$ at $\tilde{P}^2 = \mu^2$ in the solutions (12) and (13) in order to comply with the LO and NLO hadronic boundary conditions (10). Note that the moment of the NLO quark input in Eq. (7) is given by

$$q_{\rm NLO}^{\gamma(P^2),n} = 3e_q^2\frac{\alpha}{2\pi}\left[\frac{2}{n^2} - \frac{4}{(n+1)^2} + \frac{4}{(n+2)^2} - \frac{2}{n} + \frac{6}{n+1} - \frac{6}{n+2}\right]. \quad (15)$$

The LO results are of course entailed in these expressions by simply dropping all the obvious higher order terms $(\beta_1, \vec{k}^{(1)n}, \hat{U})$. For the flavor-nonsinglet case the (matrix) solutions in Eqs. (12) and (13) reduce to single equations for $\Sigma^{\gamma(P^2)} \to q_{\rm NS}^{\gamma(P^2)}$ with $\vec{k}^n \to k_{\rm NS}^n$ and $\hat{U} \to U_{\rm NS}$ expressed in terms of $P_{\rm NS}^{(0)n}$ and $P_{\rm NS}^{(1)n}$ [6]. Furthermore, the boundary conditions at $Q^2 = P^2$, given by Eq. (8), have to be implemented in the DIS$_\gamma$ scheme; therefore $k_{\rm NS}^{(1)n}$ and $\vec{k}^{(1)n} \equiv (k_q^{(1)n}, k_g^{(1)n})$ in (12) have to be taken as specified in Eq. (3.1) of Ref. [6]. Furthermore, $\alpha_s^{(f)}(Q^2)$ has to be "matched" at the $\overline{\rm MS}$ thresholds $Q = m_h$, i.e., $\alpha_s^{(f+1)}(m_h^2) = \alpha_s^{(f)}(m_h^2)$, where $f+1$ denotes the number of relevant active flavors at $Q > m_h$. On the other hand, we fix $f = 3$ in the splitting functions $P_{ij}^{(0,1)}$ in (13) for consistency since we treat the heavy quark sector $(c, b, \ldots)$ by the perturbatively stable full production cross sections in fixed-order perturbation theory, i.e., via $\gamma^* g^\gamma \to h\bar{h}$, etc., keeping $m_h \neq 0$. [If one matches f accordingly in the $P_{ij}^{(0,1)}$ as well, $g^{\gamma(P^2)}(x, Q^2)$ would be overestimated by 20–40% for the largest possible $P^2 \simeq Q^2/10$ at $Q^2 \gtrsim 100$ GeV^2, whereas the results for $q^{\gamma(P^2)}(x, Q^2)$ are far less affected; the real photon densities $g^{\gamma(P^2=0)}$ and $q^{\gamma(P^2=0)}$, on the contrary, remain practically unchanged.]

It should be noted that these distributions $f^{\gamma(P^2)}(x, Q^2)$, to be obtained from the above moments via a simple numerical Mellin inversion [6], do *not* afford any further modifications [8] of the standard expressions, e.g. Eq. (1), for the virtual photon flux when P^2 is taken, as argued above, to be $P^2 = P_{\rm min}^2$. They apply and are relevant whenever $P^2 \ll Q^2$, so as to suppress possible higher twist, i.e., $(P^2/Q^2)^n$, contributions and to guarantee, furthermore, the dominance of the transverse photon contributions to the investigated cross sections.

The photonic parton distributions discussed thus far are adequate for the light u, d, s flavors and the gluon. The production of heavy flavors $(c, b, \ldots)$ should be more adequately described, within fixed-order perturbation theory, by the appropriate production processes as will be discussed in the next section.

III. QUANTITATIVE RESULTS

The application of our P^2-smooth distributions $f^{\gamma(P^2)}(x, Q^2)$ to physical processes $eX \to eX'$ dictates an identification of the relevant $\gamma(P^2)X \to X'$ *sub*-cross-sections according to $\hat{\sigma}^{\gamma(P^2)X\to X'} = \hat{\sigma}^{\gamma X\to X'}$, where the real photon is as usual denoted by $\gamma \equiv \gamma(P^2 = 0)$. In particular the calculation of $F_{2,L}^{\gamma(P^2)}(x, Q^2)$ requires for the light quarks (u, d, s) and gluon contributions formally the *same* expressions [4] as for $P^2 = 0$:

$$\frac{1}{x}F_i^{\gamma(P^2)}(x,Q^2) = 2\sum_q e_q^2\left\{q^{\gamma(P^2)}(x,Q^2) + \frac{\alpha_s(Q^2)}{2\pi}\int_x^1\frac{dy}{y}\left[C_{q,i}\left(\frac{x}{y}\right)q^{\gamma(P^2)}(y,Q^2) + C_{g,i}\left(\frac{x}{y}\right)g^{\gamma(P^2)}(y,Q^2)\right]\right\} + \frac{1}{x}F_{i,h}^{\gamma(P^2)}(x,Q^2) + \frac{1}{x}F_{i,h}^{g^{\gamma(P^2)}}(x,Q^2) \quad (16)$$

with $i = 2, L$ and

$$C_{q,2}(z) = \frac{4}{3}\left[\frac{1+z^2}{1-z}\left(\ln\frac{1-z}{z} - \frac{3}{4}\right) + \frac{1}{4}(9+5z)\right]_+, \quad C_{q,L}(z) = \frac{8}{3}z,$$
$$C_{g,2}(z) = \frac{1}{2}\left[(z^2+(1-z)^2)\ln\frac{1-z}{z} - 1 + 8z(1-z)\right], \quad C_{g,L}(z) = 2z(1-z), \quad (17)$$

where the convolution with the $[\,]_+$ distribution can be easily calculated using, for example, Eq. (A.21) of Ref. [5]. Note that the expression for the longitudinal structure function $F_L \equiv F_2 - 2xF_1$ refers to a NLO quantity since the NLO coefficient functions are defined and obtained via $C_L \equiv C_2 - 2C_1$. The LO expression for F_2 is obviously entailed

in the above equations by simply dropping all higher order terms ($C_{q,2}, C_{g,2}, \beta_1$) in Eqs. (14) and (16). For the "direct" heavy quark contribution in Eq. (16) one should use, in the same spirit, the Bethe-Heitler process $\gamma^*(Q^2)\gamma \to h\bar{h}$ for calculating $F_{2,h}^{\gamma}$ (where $h = c, b, \ldots$), as given for example in Eq. (9) of Ref. [4], and its counterpart for F_L. The corresponding expressions with $e_h^4\alpha \to e_h^2\alpha_s/6$ are obtained for $\gamma^*(Q^2)g^{\gamma(P^2)} \to h\bar{h}$, which are relevant for the "resolved" virtual photon contributions [9]. In general, however, it is advisable in practice to keep the P^2/m_h^2 terms in the "direct" heavy quark contribution and to use instead [11], for $W^2 = (p_\gamma + q)^2 = Q^2(1 - x - xP^2/Q^2)/x \geq (2m_h)^2$:

$$\frac{1}{x}F_{2,h}^{\gamma(P^2)}(x,Q^2) = 3e_h^4\frac{\alpha}{\pi}\left\{\beta(-1+6x-6x^2) + 2x^2\left(\frac{2m_h^2 - P^2}{Q^2} - \frac{4m_h^4}{Q^4}\right)\left(\frac{1}{\beta_-} - \frac{1}{\beta_+}\right)\right.$$
$$\left. + \left[x^2 + (1-x)^2 + x(1-3x)\frac{4m_h^2}{Q^2} - x^2\frac{8m_h^4}{Q^4}\right]\ln\frac{\beta_+}{\beta_-}\right\},$$
$$\frac{1}{x}F_{L,h}^{\gamma(P^2)}(x,Q^2) = 3e_h^4\frac{4\alpha}{\pi}\left\{\beta x(1-x) - x^2\frac{2m_h^2}{Q^2}\ln\frac{\beta_+}{\beta_-}\right\} \tag{18}$$

where $\beta^2 = 1 - 4m_h^2/W^2$ and $\beta_\pm = 1 \pm \beta(1 - 4x^2P^2/Q^2)^{1/2}$. These expressions are valid [11] in the limit $2xP^2/Q^2 \ll 1$ and reduce at $P^2 = 0$ to the Bethe-Heitler expression for $\gamma^*(Q^2)\gamma \to h\bar{h}$. We have checked that for all practical purposes they reproduce to within less than 2% the far more cumbersome exact results in Appendix E of Ref. [12]. Similarly, one should also keep in practice the P^2/m_h^2 terms for calculating the "resolved" heavy quark contribution in Eq. (16) via $\gamma^*(Q^2)g^{\gamma(P^2)} \to h\bar{h}$ with $\frac{1}{x}f_{i=2,L}^{\gamma^*(Q^2)g^{\gamma(P^2)}\to h\bar{h}}(x,Q^2)$ given by Eq. (18) with $e_h^4\alpha \to e_h^2\alpha_s(\mu'^2)/6$ and thus [9]

$$F_{i,h}^{g^{\gamma(P^2)}}(x,Q^2) = \int_{z_{\min}}^{z_{\max}}\frac{dz}{z}zg^{\gamma(P^2)}(z,\mu'^2)$$
$$\times f_i^{\gamma^*(Q^2)g^{\gamma(P^2)}\to h\bar{h}}\left(\frac{x}{z},Q^2\right), \tag{19}$$

where $z_{\min} = x(1 + 4m_h^2/Q^2 + P^2/Q^2)$ and $z_{\max} = 1/(1 + P^2/Q^2)$.

Disregarding for the moment the heavy quark contributions, we present in Figs. 1 and 2 our LO and NLO results for $F_2^{\gamma(P^2)}(x,Q^2)$ by just keeping, aside from the gluon, the light u, d, s flavors. In order to demonstrate the effect of the (theoretically ill understood) nonperturbative contributions, we plot also the purely perturbative results which correspond to setting $\eta(P^2) \equiv 0$ in Eq. (8). At $Q^2 = 10$ GeV^2 the nonperturbative (VMD) component is important throughout the whole x region shown in Fig. 1. At $P^2 = 10$ GeV^2 (i.e., $P^2 \gg \Lambda^2$) and $Q^2 = 100$ GeV^2 (i.e., $Q^2 \gg P^2$), shown in Fig. 2, this nonperturbative VMD component is still important in the small-x region despite $P^2 \gg m_\rho^2$! In the larger x region ($x \gtrsim 0.01$), however, the perturbative component dominates when $P^2 \gg m_\rho^2$. It is only for $P^2 \ggg m_\rho^2$, e.g., $P^2 = 10^2$ GeV$^2 \ll Q^2 = 10^3$ GeV^2, when the nonperturbative component becomes entirely negligible (on a few percent level) for $x \geq 10^{-4}$ as compared to the perturbative one. The distinct differences between LO and NLO results in Figs. 1 and 2 at $x \gtrsim 10^{-3}$ are mainly due to the different perturbative NLO input in Eq. (7) which does not exist for the real ($P^2 = 0$) photon structure. For comparison we also show the NLO predictions for the real photon $P^2 = 0$. It should be furthermore noted that the virtual photon structure function and parton distributions are kinematically constrained within [2] $0 \leq x \leq (1 + P^2/Q^2)^{-1}$.

Since the purely perturbative ($\eta \equiv 0$) component of $\gamma(P^2)$ is uniquely calculable, a detailed measurement of the x and P^2 dependence at various fixed values of Q^2, as shown in Figs. 1 and 2 would shed light on the theoretically far less understood nonperturbative ($\eta \neq 0$) contributions in Eqs. (8)–(10) and eventually establish the absolute perturbative QCD predictions. The only

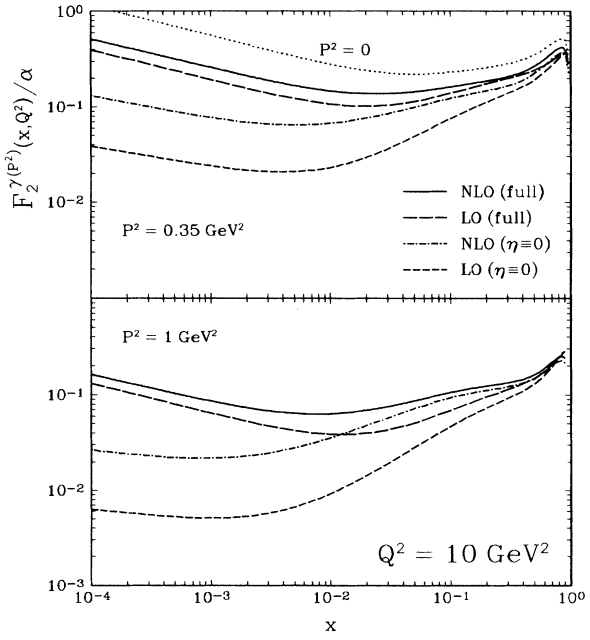

FIG. 1. LO and NLO predictions for the x dependence of the virtual photon structure function $F_2^{\gamma(P^2)}$ at $Q^2 = 10$ GeV^2 and various fixed values of $P^2 \ll Q^2$, neglecting any heavy quark contribution. The purely perturbative results correspond to the curves with $\eta \equiv 0$ in Eq. (8). For comparison, the dotted curve shows the NLO prediction for a real photon ($P^2 = 0$).

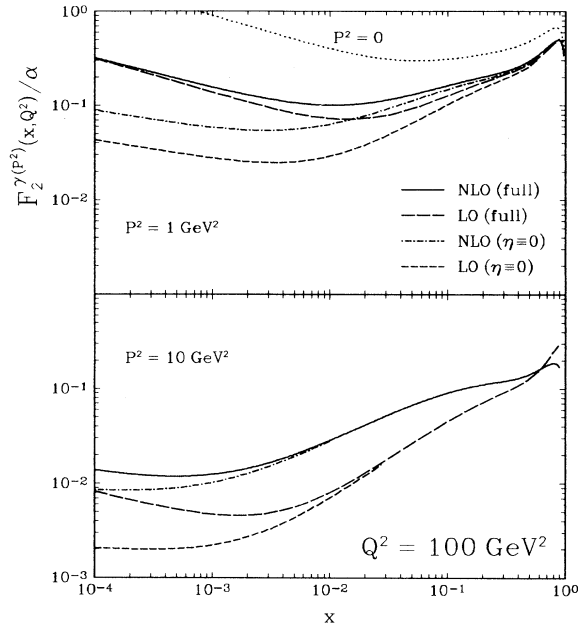

FIG. 2. As in Fig. 1 but at $Q^2 = 100$ GeV^2.

measurement [13] of the virtual photon structure function available thus far is compared in Fig. 3 with our NLO prediction for $F_{\rm eff} \equiv F_2 + \frac{3}{2}F_L$ which is the combination of structure functions measured effectively by the PLUTO experiment [13], i.e., $d\sigma/dx\,dy \sim (1-y)F_{\rm eff} + O(y^2)$ for the double-tagged events in the PLUTO kinematic region. Because of the poor statistics of the limited PLUTO data [13], our full NLO QCD predictions cannot be distinguished, for the time being, from the naive (i.e., not resummed) "box" expectations [13] shown by the dotted curve in Fig. 3. This box result consists of two pieces:

$$F_{\rm box}^{\gamma(P^2)}(x,Q^2) = F_{\rm QPM}^{\gamma(P^2)} + F_{\rm VMD}^{\gamma(P^2)}, \qquad (20)$$

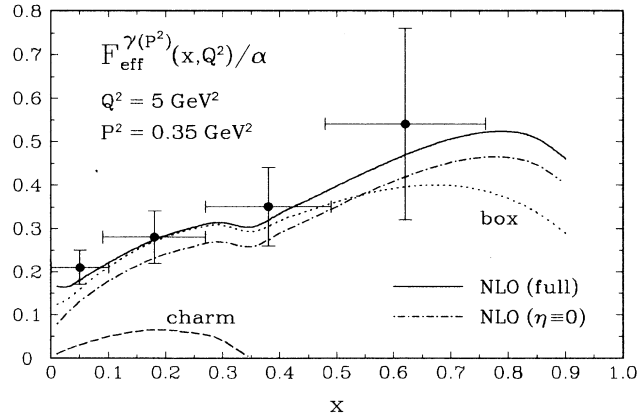

FIG. 3. NLO predictions for $F_{\rm eff}^{\gamma(P^2)} \equiv F_2 + \frac{3}{2}F_L$. The charm contribution has been calculated according to Eq. (18), using $m_c = 1.5$ GeV, and the box is defined in Eq. (20). The PLUTO data are taken from Ref. [13]. The purely perturbative results correspond to $\eta \equiv 0$ in Eq. (8).

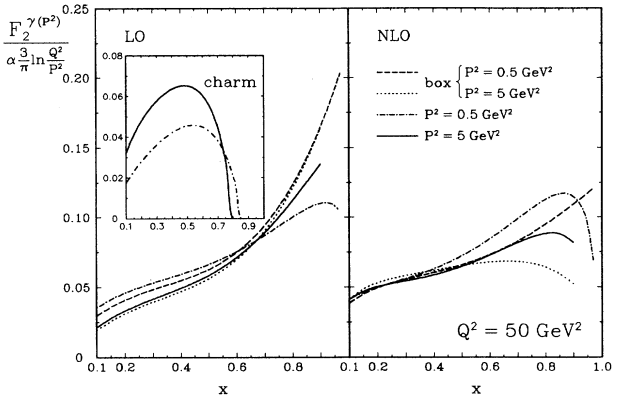

FIG. 4. LO and NLO predictions for the x-dependence of $F_2^{\gamma(P^2)}(x,Q^2)$ at $Q^2 = 50$ GeV^2 and for increasing values of P^2. For comparing with future $P^2 \neq 0$ measurements, the charm contribution according to Eq. (18), as shown in the inset, has to be added to the LO and NLO predictions. The box is defined in Eqs. (20) and (21), where the additional "finite" x-dependent terms in the curly brackets of (20) contribute only in NLO.

where $F_{\rm QPM}$ refers to the standard QPM-box result, which for the light u, d, s flavors is given by [1,2] [cf. Eq. (7)]

$$\frac{1}{x}F_{2,\rm QPM}^{\gamma(P^2)}(x,Q^2) = 3\sum_q e_q^4 \frac{\alpha}{\pi}\left\{[x^2+(1-x)^2]\ln\frac{Q^2}{P^2}\right.$$
$$+[x^2+(1-x)^2]\ln\frac{1}{x^2} - 2$$
$$\left.+6x-6x^2\right\},$$
$$\frac{1}{x}F_{L,\rm QPM}^{\gamma(P^2)}(x,Q^2) = 3\sum_q e_q^4 \frac{\alpha}{\pi}4x(1-x), \qquad (21)$$

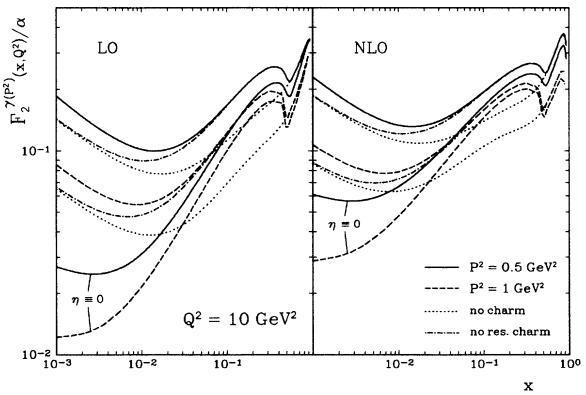

FIG. 5. LO and NLO predictions for $F_2^{\gamma(P^2)}(x,Q^2)$ at $Q^2 = 10$ GeV^2 and for different fixed values of $P^2 \ll Q^2$. The purely perturbative contributions correspond to $\eta \equiv 0$ [in Eq. (8)]. The dotted curves refer to the total ($\eta \neq 0$) results with the charm contribution being omitted, while the dashed-dotted curves correspond to the ones where only the "direct" charm contribution, Eq. (18), has been taken into account, i.e., where the "resolved" $[\gamma^*(Q^2)g^{\gamma(P^2)} \to c\bar{c}]$ charm contribution has been omitted.

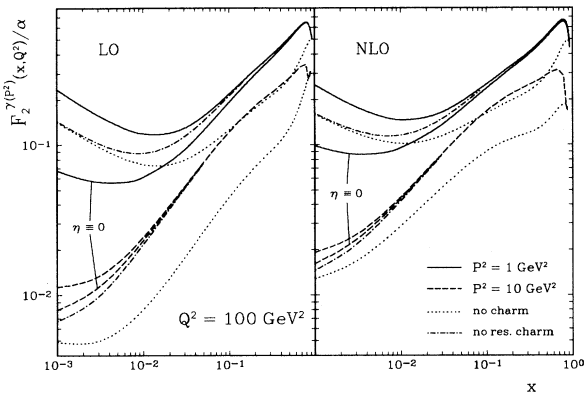

FIG. 6. As in Fig. 5 but for $Q^2 = 100$ GeV^2.

and for the heavy quarks $(c, b, \ldots)$ by Eq. (18); the nonperturbative VMD contribution in (20) is calculated according to the input at $Q^2 = P^2$, i.e., the first term on the RHS of Eq. (8) together with Eq. (10). Note that in

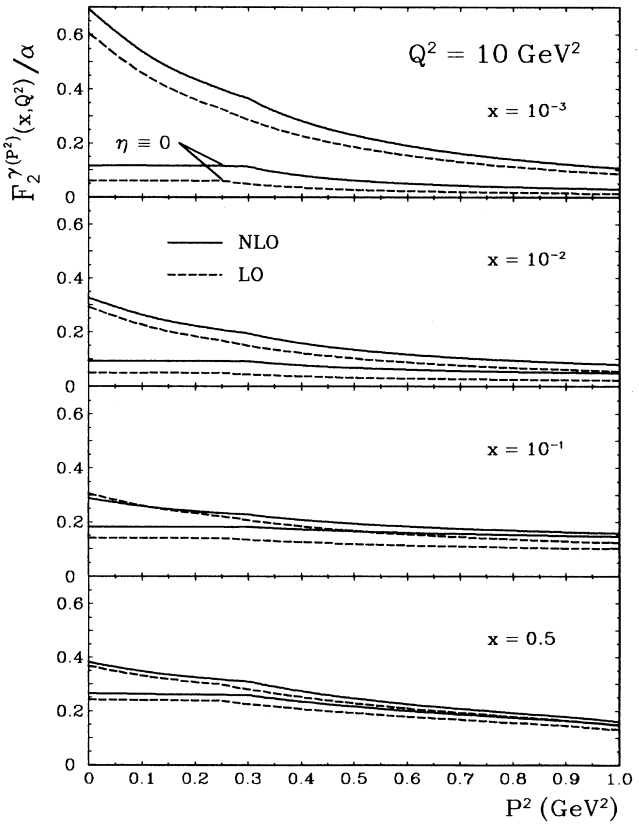

FIG. 7. LO and NLO predictions for the P^2 dependence of $F_2^{\gamma(P^2)}(x, Q^2)$ at $Q^2 = 10$ GeV^2 for various fixed values of x. The "direct" and "resolved" [9] charm contributions are included according to Eqs. (18) and (19), respectively. The purely perturbative LO and NLO contributions are, for each value of x, shown by the lower lying pair of LO and NLO curves corresponding to $\eta \equiv 0$ [in Eq. (8)].

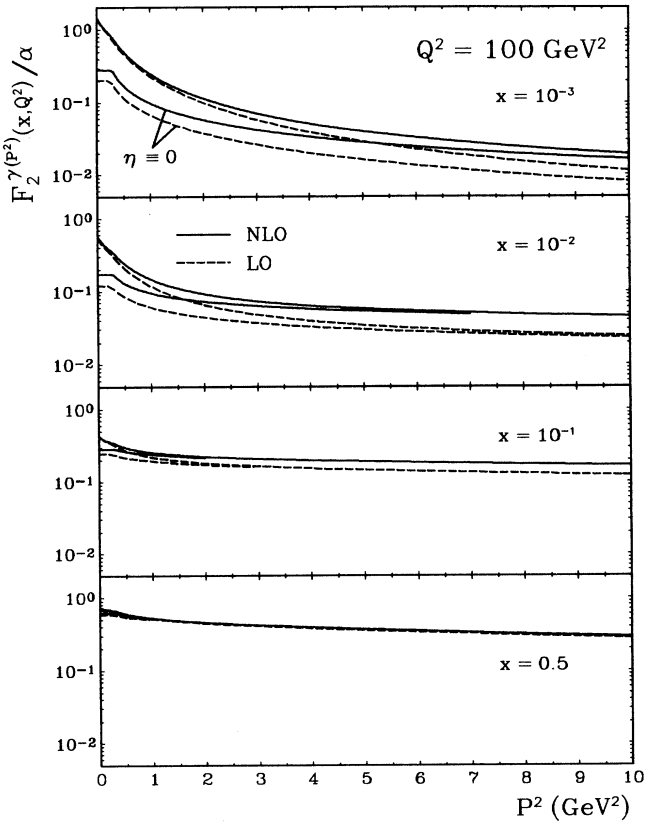

FIG. 8. As in Fig. 7 but at $Q^2 = 100$ GeV^2.

LO it is only the first logarithmic term in curly brackets in (21) which contributes.

In Fig. 4 we show some representative LO and NLO predictions for $F_2^{\gamma(P^2)}(x, Q^2 = 50\ \text{GeV}^2)$ in the medium-to-large x region. As P^2 increases, the LO QCD predic-

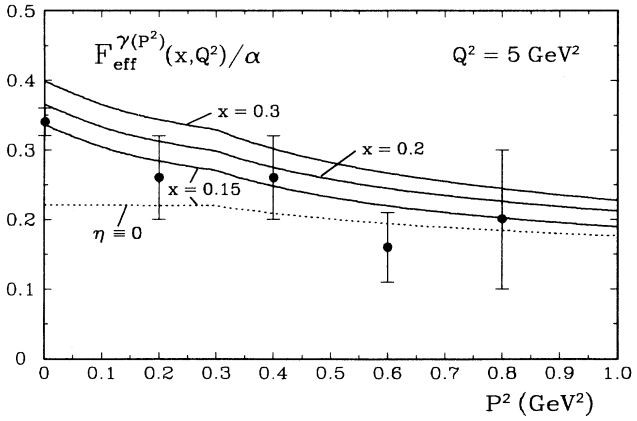

FIG. 9. NLO predictions for the P^2 dependence of $F_{\text{eff}}^{\gamma(P^2)}(x, Q^2) \equiv F_2 + \frac{3}{2}F_L$ at $Q^2 = 5$ GeV^2 and for $x = 0.15, 0.2, 0.3$ corresponding to a representative range of average x values covered by the Q^2- and x-averaged PLUTO data [13], which are shown for illustration. The purely perturbative prediction corresponds to $\eta \equiv 0$ in Eq. (8).

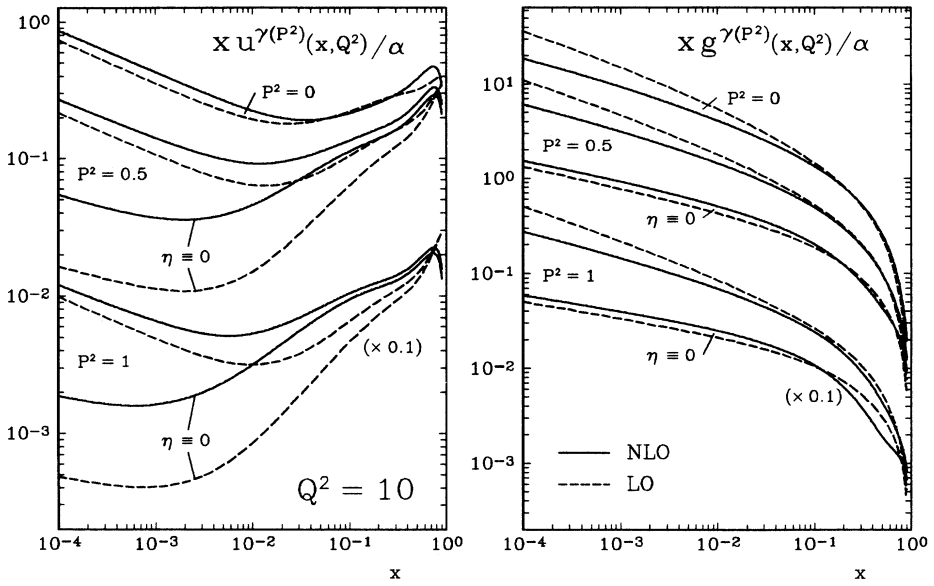

FIG. 10. LO and NLO predictions for the up and gluon distributions of a virtual photon $\gamma(P^2)$ at $Q^2(\mathrm{GeV}^2) = 10$ and various fixed values of $P^2(\mathrm{GeV}^2)$. The purely perturbative results have been derived from Eq. (8) for $\eta \equiv 0$. The DIS_γ results for $u^{\gamma(P^2)}$ can be easily converted to the $\overline{\mathrm{MS}}$ scheme with the help of Eq. (4), whereas $g^{\gamma(P^2)}$ remains the same in both schemes. The results at the largest value of P^2 shown have been multiplied by 0.1. For comparison, the LO and NLO predictions for the parton distributions of the real photon ($P^2 = 0$) [4] are shown as well.

tions approach [14] the box results, defined by Eqs. (20) and (21), as they should in the large-x region since there is less gluon radiation the more P^2 approaches Q^2. In NLO such a naive comparison is not very sensible any more due to the large NLO box expression [where the "finite" x-dependent terms in Eq. (21) enter] as shown in Fig. 4. The (direct) charm contribution given by Eq. (18), is shown in the inset of Fig. 4 and should be added to the LO and NLO predictions of $F_2^{\gamma(P^2)}$ for a realistic comparison with future experiments. In Figs. 5 and 6 we present our full realistic (i.e., including charm) predictions for $F_2^{\gamma(P^2)}(x, Q^2)$ also for the very small-x region which will be relevant for future LEP measurements. The charm contribution, calculated via the direct and resolved expressions (18) and (19), respectively, is sizable throughout most of the relevant kinematic regions shown in Figs. 5 and 6 as can be inferred from the dotted curves which represent the respective total results without charm. The direct charm contribution is important in the larger x region ($x \gtrsim 10^{-2}$), which can be inferred from the dashed-dotted curves where the resolved charm contribution, Eq. (19), has not been added. These curves also demonstrate, when compared with the full results (solid and dashed curves in Figs. 5 and 6) that the resolved charm contribution [9] becomes relevant only in the small-x region ($x \lesssim 10^{-2}$). Furthermore, as noticed already in Figs. 1 and 2, the nonperturbative VMD component is important and partly even dominates over the purely perturbative contribution, corresponding to $\eta \equiv 0$ in Eq. (8), as shown in Figs. 5 and 6; only for

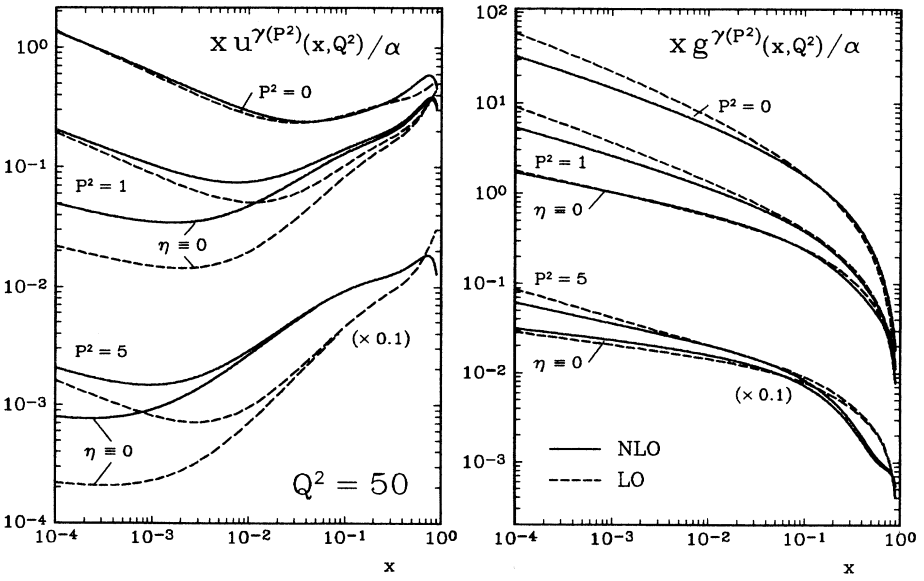

FIG. 11. As in Fig. 10 but at $Q^2(\mathrm{GeV}^2) = 50$.

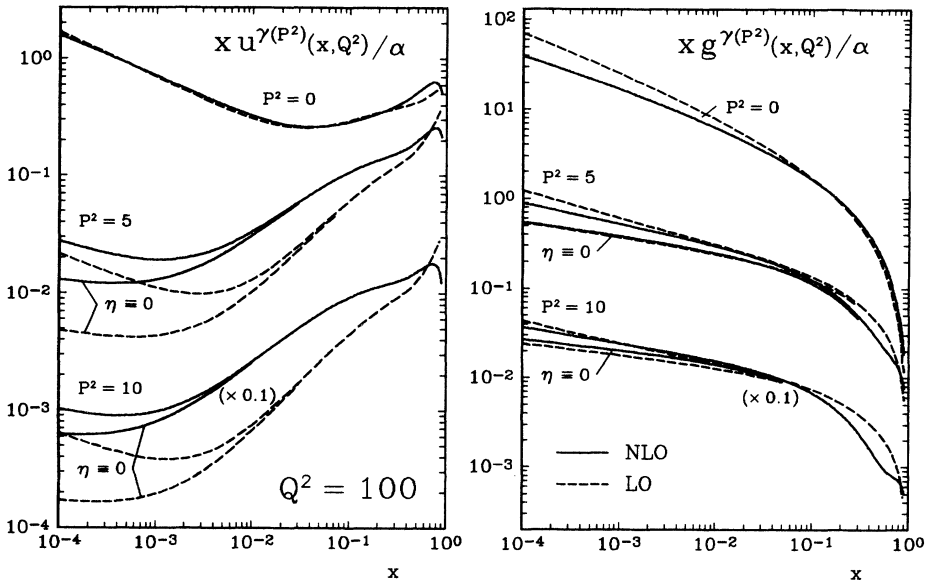

FIG. 12. As in Fig. 10 but at $Q^2(\mathrm{GeV}^2) = 100$.

$P^2 \gtrsim 10$ GeV^2 and $x \gtrsim 10^{-3}$ does the nonperturbative contribution become marginal as can be inferred from Fig. 6.

Our LO and NLO predictions for the P^2 dependence of $F_2^{\gamma(P^2)}(x, Q^2)$, which extrapolates *smoothly* to the *real* ($P^2 = 0$) photon case due to our boundary conditions (8) and (10), are shown in Figs. 7 and 8 which will be relevant for future LEP experiments. Besides the direct charm contribution, Eq. (18), the additional charm contribution stemming from the resolved photon component [9] and calculated via $\gamma^*(Q^2)g^{\gamma(P^2)} \to c\bar{c}$, Eq. (19), has been included in Figs. 7 and 8. As has been shown already in Figs. 5 and 6, these latter resolved component contributes only in the small-x region ($x \lesssim 10^{-2}$). Furthermore, as $P^2 \to 0$, the nonperturbative VMD component in (8) dominates in particular at small values of $x, x \lesssim 10^{-2}$, as can be inferred from the purely perturbative $\eta \equiv 0$ results in Figs. 7 and 8. Note that the increase of our total results below $P^2 \leq \mu^2 = 0.25 - 0.3$ GeV^2 is entirely due to the increase of $\eta(P^2)$, as $P^2 \to 0$, in Eq. (8) and (9). Our ansatz in Eqs. (8)–(10) for this important nonperturbative contribution appears to be indeed reasonable when compared with the P^2 dependence of $F_{\mathrm{eff}}^{\gamma(P^2)}(x, Q^2)$, $F_{\mathrm{eff}} \equiv F_2 + \frac{3}{2}F_L$, as measured by the PLUTO experiment [13]. Although we cannot directly compare with the PLUTO data, which have been averaged [13] over both x and Q^2, they lie within our predictions for $0.15 \leq x \leq 0.3$ shown in Fig. 9 corresponding

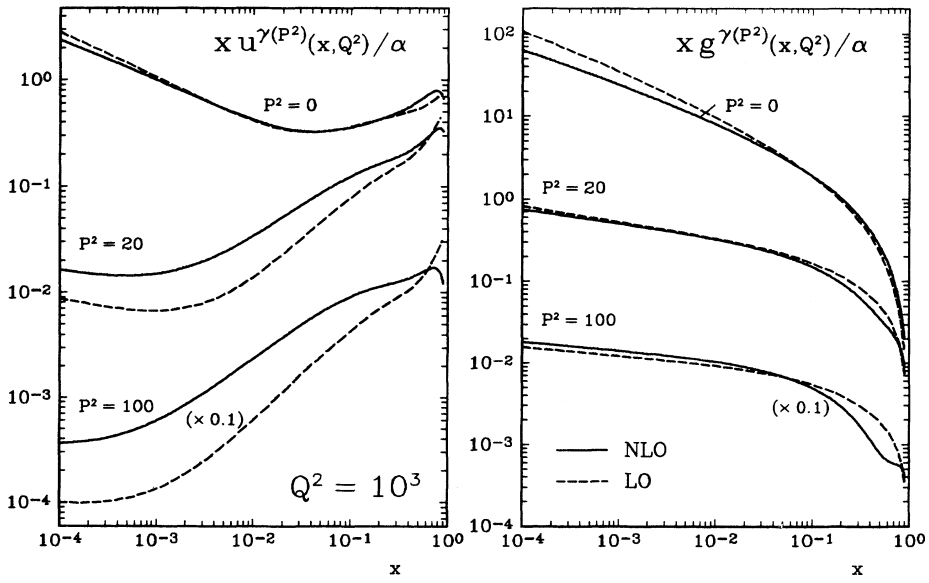

FIG. 13. As in Fig. 10 but at $Q^2(\mathrm{GeV}^2) = 10^3$. Here, the purely perturbative ($\eta \equiv 0$) results are entirely dominant and practically coincide with the full ($\eta \neq 0$) results shown.

to the averaged x values at $Q^2 = 5$ GeV^2 of the PLUTO experiment. It should be emphasized that this agreement does not only refer to the observed P^2 dependence, but to the absolute normalization as well.

Finally, our predictions for the parton distributions of a virtual photon $u^{\gamma(P^2)}(x,Q^2)$ and $g^{\gamma(P^2)}(x,Q^2)$ are presented in Figs. 10–13. With $g^{\gamma(P^2)}$ being the same in the DIS$_\gamma$ and $\overline{MS}$ scheme, the results for $u^{\gamma(P^2)}$ are shown in the DIS$_\gamma$ scheme which can be easily transformed to the $\overline{MS}$ scheme by simply subtracting, according to Eq. (4), $\delta u^\gamma(x)$ as defined in Eq. (5). (For actual NLO calculations the $\overline{MS}$ distributions might be more convenient [6] since most NLO partonic subprocesses have been calculated in the $\overline{MS}$ scheme.) It can be inferred from the purely perturbative ($\eta \equiv 0$) contributions that the nonperturbative components, entering for $\eta \neq 0$ in Eq. (8), are non-negligible and partly even dominant. Only for $P^2 (\ll Q^2)$ larger than about 10 GeV^2 does the perturbative component start to dominate, as can be seen from Figs. 12 and 13. These results should be of particular interest for present HERA $ep \to eX$ measurements, i.e., $\gamma(P^2)p \to X$, where now the scale Q in $f^{\gamma(P^2)}(x,Q^2)$ refers to some properly chosen scale of the produced hadronic system X, e.g., $Q \sim p_T^{\rm jet}$ in high-p_T jet events ($p_T^2 \gg P^2$), etc.

IV. DISCUSSION AND CONCLUSIONS

The main purpose of the present paper was to formulate a consistent set of boundary conditions at $Q^2 = P^2$ which allow for a calculation of the virtual photon structure functions $F_{2,L}^{\gamma(P^2)}(x,Q^2)$ and the parton distributions $f^{\gamma(P^2)}(x,Q^2), f = q, \bar{q}, g$, also in the next-to-leading order of QCD *as well as* for a *smooth* transition to $P^2 = 0$, i.e., to the structure functions of a real photon. The obtained results and predictions therefore apply uniformly to *all* $P^2 \geq 0$ whenever $\gamma(P^2)$ is probed at a scale $Q^2 \gg P^2$, so as to suppress possible higher twist, i.e., $(P^2/Q^2)^n$, contributions. Thus one might naively expect that for $\Lambda^2 \ll P^2 \ll Q^2$ the virtual photonic parton distributions should be uniquely perturbatively calculable from first principles in LO and NLO, in contrast to the parton distributions of a real ($P^2 = 0$) photon. It turned out, however, that the nonperturbative (VMD) components are important and non-negligible, even at $P^2 \gg m_\rho^2$, for most values of Q^2, P^2, and x of present interest. [It should be emphasized that these nonperturbative components, $\eta(P^2)$ and $f_{\rm nonpert}^{\gamma(P^2)}$ in Eq. (8), represent the largest uncertainty in our quantitative results and have eventually to be tested by future experiments.] For example, at $Q^2 = 100$ GeV^2 and $P^2 \gtrsim 5$ GeV^2 the purely perturbative component dominates only in the large-x region ($x \gtrsim 0.01$). Only for $P^2 \gtrsim 20$ GeV^2, and consequently $Q^2 \gtrsim 500$ GeV^2, the nonperturbative component becomes entirely negligible as long as $x \gtrsim 10^{-4}$. Our detailed LO and NLO predictions for $F_2^{\gamma(P^2)}(x,Q^2)$ should become important for future e^+e^- experiments at LEP; the ones for $f^{\gamma(P^2)}(x,Q^2)$ should be of particular interest for present HERA $ep \to eX$ measurements, i.e., $\gamma(P^2)p \to X$, where now the scale Q refers to some properly chosen scale of the produced hadronic system X, e.g., $Q^2 \sim (p_T^{\rm jet})^2 \gg P^2$, etc., as mentioned previously.

For P^2 approaching $Q^2, P^2 \simeq Q^2$, the virtual photon $\gamma(P^2)$ is expected to contribute merely as a pointlike particle without any further universal partonic content. Therefore its detailed contribution will be process dependent in the usual way: For example, $e^+e^- \to e^+e^-X$ should be simply described by the full QPM box $\gamma^*(Q^2)\gamma(P^2) \to q\bar{q}$ with all higher twist, i.e., $(P^2/Q^2)^n$, terms kept. Since the full perturbative $O(\alpha_s)$ corrections to this virtual box have not been calculated yet, it is not possible, for the time being, to determine reliably at what values of P^2 (and possibly x) this $O(\alpha_s)$ corrected virtual box becomes the more appropriate and correct description. Similar remarks hold for a deep inelastic process $ep \to eX$, i.e., $\gamma(P^2)p \to X$, where $O(\alpha_s)$ corrections to pointlike virtual $\gamma(P^2)$-parton subprocesses have to be analyzed in detail in order to decide at what scale P^2 these pointlike expressions become the more appropriate description and the virtual photonic parton distributions (i.e., resummations) become irrelevant.

ACKNOWLEDGMENTS

This work has been supported in part by the Bundesministerium für Forschung und Technologie, Bonn.

[1] T. Uematsu and T. F. Walsh, Nucl. Phys. **B199**, 93 (1982).
[2] G. Rossi, Phys. Rev. D **29**, 852 (1984); UC San Diego Report No. UCSD-10P10-227 (unpublished).
[3] S. Frixione, M. L. Mangano, P. Nason, and G. Ridolfi, Phys. Lett. B **319**, 339 (1993), and references therein.
[4] M. Glück, E. Reya, and A. Vogt, Phys. Rev. D **46**, 1973 (1992).
[5] M. Glück, E. Reya, and A. Vogt, Z. Phys. C **53**, 651 (1992).
[6] M. Glück, E. Reya, and A. Vogt, Phys. Rev. D **45**, 3986 (1992).
[7] W. Ibes and T. F. Walsh, Phys. Lett. B **251**, 450 (1990).
[8] F. M. Borzumati and G. A. Schuler, Z. Phys. C **58**, 139 (1993); P. Aurenche, J.-Ph. Guillet, M. Fontannaz, Y. Shimizu, J. Fujimoto, and K. Kato, Prog. Theor. Phys. **92**, 175 (1994); M. Drees and R. M. Godbole, Phys. Rev. D **50**, 3124 (1994).
[9] The "resolved" contributions should be included only for $P^2 \ll \mu'^2$; the scale in the virtual photonic gluon distribution $g^{\gamma(P^2)}(x,\mu'^2)$ should be preferably $\mu'^2 = 4m_h^2$ irrespective of Q^2 (Ref. [10]), although a consistent LO and NLO analysis of deep inelastic ep scattering gives similar results for the choice $\mu'^2 = Q^2 + 4m_h^2$ (Ref. [10]). For the

kinematic regions considered, we adopt, for practical reasons, $\mu'^2 = Q^2 + 4m_h^2$. Although this choice is somewhat arbitrary, it affects our predictions for $F_2^{\gamma(P^2)}(x, Q^2)$ only in the very small-x region.

[10] M. Glück, E. Reya, and M. Stratmann, Nucl. Phys. **B422**, 37 (1994).

[11] C. T. Hill and G. G. Ross, Nucl. Phys. **B148**, 373 (1979).

[12] V. M. Budnev, I. F. Ginzburg, G. V. Meledin, and V. G. Serbo, Phys. Rep. **15**, 181 (1975).

[13] PLUTO Collaboration, Ch. Berger *et al.*, Phys. Lett. **142B**, 119 (1984).

[14] T. Uematsu and T. F. Walsh, Phys. Lett. **101B**, 263 (1981).